

AD-A149 389

GENERATION OF ALFVEN WAVES DUE TO THERMAL MODULATION OF  
THE ELECTRICAL CO. (U) CALIFORNIA UNIV LOS ANGELES  
CENTER FOR PLASMA PHYSICS AND FUS. M M SHOURI ET AL.

1/1

UNCLASSIFIED

NOV 84 PPG-830 N00014-76-C-0476

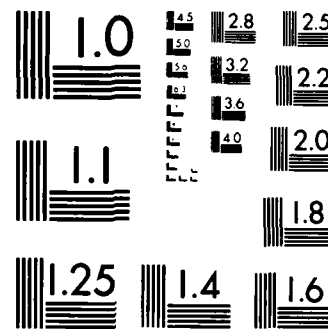
F/G 20/9

NL

END

FILED

DTIC



MICROCOPY RESOLUTION TEST CHART  
NATIONAL BUREAU OF STANDARDS 1963-A

DTIC FILE COPY

AD-A149 389



1

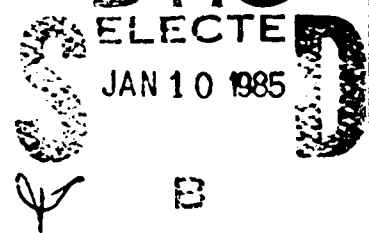
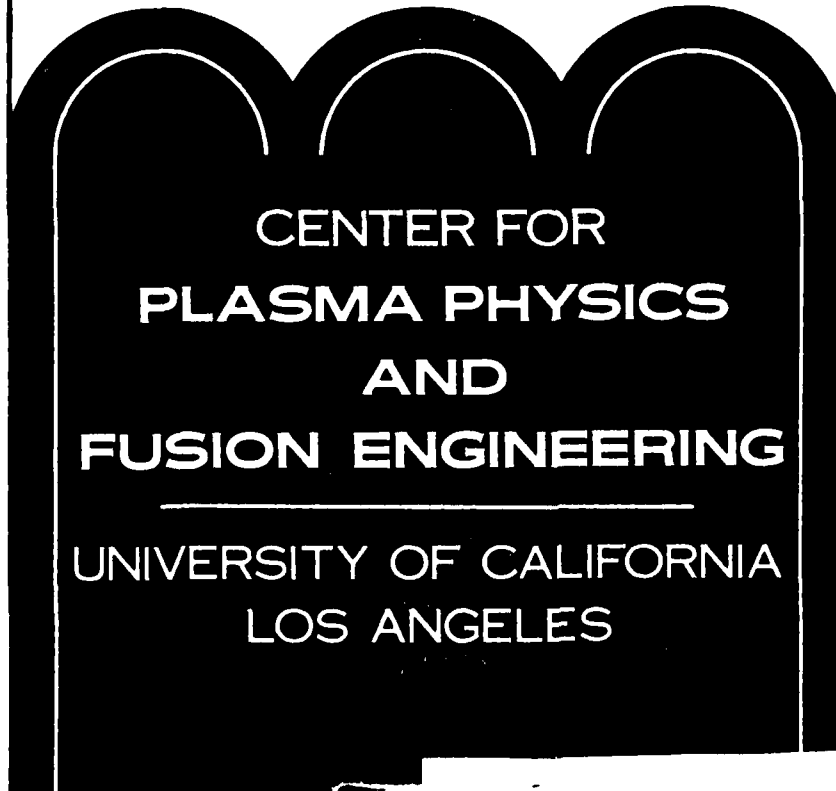
Generation of Alfven Waves due to Thermal  
Modulation of the Electrical Conductivity

M. M. Shoucri, G. J. Morales  
& J. E. Maggs

PPG-830

November, 1984

Contract N00014-76-C-0476  
NR-012-306



DISTRIBUTION STATEMENT A  
Approved for public release  
Distribution Unlimited

Generation of Alfven Waves due to Thermal  
Modulation of the Electrical Conductivity

M. M. Shoucri, G. J. Morales  
& J. E. Maggs

PPG-830

November, 1984

Contract N00014-76-C-0476  
NR-012-306

Department of Physics  
University of California  
Los Angeles, California 90024

DTIC  
ELECTE  
S JAN 10 1985 D  
B

DISTRIBUTION STATEMENT A  
Approved for public release  
Distribution Unlimited

ABSTRACT

An analytic study is made of the effects produced by a localized modulation of the electrical conductivity of a magnetized plasma carrying a field aligned current. The modulation is assumed to be caused by a heating source external to the plasma. The formulation used is applicable to modulation frequencies  $\omega$  below the ion cyclotron frequency  $\omega_{ci}$  and permits the calculation of the radiation pattern which contains shear as well as compressional Alfvén modes, and near fields. For  $\omega/\omega_{ci} \ll 1$ , the radiation appears primarily in the form of a highly collimated shear mode travelling along the field lines passing through the spot where the modulation occurs.

Accession For  
NTIS GRADE  
DTIC TAB  
Unclassified  
Justification  
**PER LETTER**  
By \_\_\_\_\_  
Date \_\_\_\_\_  
Assistant \_\_\_\_\_  
Editor \_\_\_\_\_  
Dist \_\_\_\_\_  
A-1



## I. Introduction

A possible method of exciting low frequency electromagnetic waves consists of the external remote modulation of zero order current systems flowing in magnetized plasmas. The motivation for taping internal currents is that the dimensions of external antennas required for low frequencies are prohibitively large. A significant shortening of the effective length of antennas formed inside a plasma results from the density dependence of the Alfvén speed, i.e.,  $v_A = B_0/(4\pi MN)^{1/2}$  where  $B_0$  is the confining magnetic field,  $M$  is the ion mass, and  $N$  the plasma density. The characteristic dimensions of an antenna that excites an Alfvén wave in-situ is shortened from the vacuum value by a factor  $n_A = c/v_A = \omega_{pi}/\omega_{ci}$ , where  $n_A$  is the Alfvén index of refraction,  $\omega_{pi}$  is the ion plasma frequency,  $\omega_{ci}$  is the ion cyclotron frequency, and  $c$  is the speed of light. Over a broad class of plasmas, both in the laboratory and naturally occurring, this shrinkage ranges from a factor of 10 to  $10^3$ .

Although there is a clear attractiveness in this method with regard to antenna size, the radiation efficiency and directionality of the radiated signals must be carefully examined in order to assess the overall usefulness of this scheme. It is the purpose of the present analytical study to address these issues by calculating the radiation pattern resulting from the thermal modulation of a current system frequently found in plasmas.

Specifically, this study considers the external modulation of the electrical conductivity of a collisional plasma carrying a steady ohmic current along the confining magnetic field, i.e., a field aligned current. The thermal modulation is assumed to be periodic with frequency  $\omega < \omega_{ci}$ ; it is envisioned that the thermal modulation arises due to a high frequency electron heating source with frequency  $\omega_{rf} \gg v_e$ , where  $v_e$  is the effective electron collision frequency.

In practice,  $\omega_{rf}$  would be near one of the typical electron RF heating frequencies, i.e., the electron plasma frequency  $\omega_{pe}$  or electron cyclotron frequency  $\omega_{ce}$ . In the present study we do not address the issue of thermal transport associated with the heater wave at  $\omega_{rf}$ . It is simply assumed that a localized hot spot of Gaussian shape is formed at some point in an otherwise uniform plasma. This choice of a profile simplifies the analysis and is qualitatively consistent with a detailed heat transport study previously performed by these authors for the high latitude ionosphere.<sup>1</sup>

One of the features of the present analysis is that in calculating the radiation of Alfvén waves no expansion in  $\omega/\omega_{ci}$  is made. This implies that the relative efficiency for radiating the shear Alfvén mode and the compressional Alfvén mode (which are simultaneously generated) is found. For  $\omega/\omega_{ci} \approx 0.2$  nearly 90% of the radiated power appears in the form of a shear Alfvén mode which travels along the magnetic flux tube passing through the hot spot. The compressional Alfvén mode carries away the remaining 10% in a quadrupole-like pattern that moves out of the flux tube containing the shear mode. The efficiency of the process is of the order of  $10^{-5}$ , which is quite low on absolute standards, but may result in detectable signals for the auroral ionosphere.

The principal results of the study are as follows. The radiation pattern due to modulation of the electrical conductivity is found for  $\omega/\omega_{ci} < 1$ . It contains a shear wave, a compressional wave, and near fields. The shear Alfvén mode dominates and results in a headlight radiation pattern. The low frequency highly directive wave electric fields are of the order of  $(\Delta T_e/T_e)E_0$  where  $E_0$  is the zero order dc field driving the field aligned current, and  $\Delta T_e/T_e$  is the fractional modulation of the electron temperature.

The manuscript is organized as follows. In Sec. II, the plasma model is

described and the radiation fields are calculated. Various parameter dependences of the radiation pattern are discussed in Sec. III, and conclusions are presented in Sec. IV.

## II. Analysis

Consider an infinite, uniform, collisional plasma in which a zero order steady current density  $J_{0z}$  flows along a uniform magnetic field  $B_{0z}$ . An external high frequency source of carrier frequency  $\omega_{rf}$  is amplitude modulated at a low frequency  $\omega$  such that the following frequency ordering holds

$$\nu_i \ll \omega < \omega_{ci} \ll \nu_e \ll \omega_{pi} \ll \omega_{rf} \sim \omega_{ce}, \omega_{pe} \quad (1)$$

In here  $\nu_i$  represents the ion collision frequency, and  $\nu_e = \nu_{ei}(T_e) + \nu_{en}(T_e)$  is the total effective collision frequency for electrons due to collisions with ions ( $\nu_{ei}$ ) and with neutrals ( $\nu_{en}$ ), both of which depend on the electron temperature  $T_e$ . The amplitude modulated high frequency source is assumed to produce a periodic variation in  $T_e$  whose magnitude enters into the present study as an input, but which in general must be obtained from an appropriate heat transport calculation. The  $T_e$  modulation is assumed to be spatially localized with a Gaussian shape having widths  $d_{\parallel}$  and  $d_{\perp}$  in the directions parallel and perpendicular to the magnetic field, respectively. Spatial localization of the modulation in  $T_e$  can in practice be brought about by focusing the high frequency source through appropriate external antennas or by using natural resonances or cut offs of the plasma (e.g.,  $\omega_{rf} \sim \omega_{pe}, \omega_{ce}$ ).

The sinusoidal temporal variation in  $T_e$  gives rise to an equivalent variation in the electrical conductivity tensor. For the ordering indicated in Eq. (1), the principal effect is to change the component parallel to the magnetic field giving  $\Delta\sigma_z \approx -\sigma_{zo}(\Delta\nu_e/\nu_e) \sim \sigma_{zo}(\Delta T_e/T_e)$ . We express this

variation in the form

$$\left( \frac{\Delta \sigma_z}{\sigma_{z0}} \right) = \left( \frac{\Delta \sigma_z}{\sigma_{z0}} \right)_m f(x, y, z) e^{-i\omega t} + \text{c.c.}, \quad (2)$$

where  $f(x, y, z) = \exp [-(x^2 + y^2)/d_{\perp}^2 - z^2/d_{\parallel}^2]$ ,  $\sigma_{z0} = (\omega_{pe}^2/4\pi v_e)$  is the unperturbed value of the parallel conductivity,  $(\Delta \sigma_z/\sigma_{z0})_m$  is the maximum modulation, and  $x, y, z$  form a mutually orthogonal coordinate system with  $(x, y)$  representing the coordinates perpendicular to the magnetic field. It is assumed that the conductivity exhibits a modulation at the same frequency  $\omega$  as the temperature. The resulting physical configuration is schematically indicated in Fig. 1 where, in addition, the dominant field pattern of the radiated Alfvén wave is shown.

In general, the thermal modulation produces a modulation in current density given by  $\Delta \underline{J} = \underline{J} \exp(-i\omega t) + \text{c.c.}$ , with

$$\underline{J} = \tilde{\sigma}(\omega) \cdot \underline{E} + \Delta \sigma_z \underline{E}_0 \hat{z} + \tilde{\sigma}_e \cdot \nabla \left( \frac{\Delta T_e}{e} \right) - \left( \frac{e E_0 \hat{z}}{4\pi m v_e} \right) \nabla \cdot \underline{E} \quad , \quad (3)$$

where  $e$  and  $m$  refer to the electron charge and mass,  $E_0$  is the zero order dc electric field responsible for sustaining the field aligned current, and  $\tilde{\sigma}(\omega) = \tilde{\sigma}_e + \tilde{\sigma}_i$  is the complex conductivity tensor due to electron ( $\tilde{\sigma}_e$ ) and ion ( $\tilde{\sigma}_i$ ) contributions. In Eq.(3)  $\underline{E}$  refers to the self-consistent electric field at frequency  $\omega$  generated by the plasma in response to the change in temperature  $\Delta T_e$ . The effect of  $\underline{E}$  appears in two forms: 1) through the usual dielectric response represented by  $\tilde{\sigma}(\omega) = (i\omega/4\pi)(\tilde{I} - \tilde{\epsilon})$  with  $\tilde{\epsilon}$  the dielectric tensor; 2) as a space charge bunching due to the pile up of flowing electrons, and represented by the  $\nabla \cdot \underline{E}$  term. The third term in Eq.(3) is the effect of the thermo-electric modulation.

We shall show that the last two terms in Eq.(3) can be made negligible

ion our problem and we will only use the current due to the ohmic modulation as source. Eq.(3) is then rewritten as the sum of the wave dielectric and the source contributions

$$\underline{J} \approx \tilde{\sigma}(\omega) \cdot \underline{E} + \Delta\sigma_z E_0 \hat{z} . \quad (3a)$$

Since the charge bunching term arises due to motion parallel to the magnetic field, its effect is identical to that in an unmagnetized plasma, i.e., it contributes a correction to the  $\Delta\sigma_z E_0 \hat{z}$  source in Eq. (3) of order  $(\lambda_d/\lambda_t)^2$ , where  $\lambda_d = (c^2/4\pi\omega\sigma_{z0})^{1/2}$  is the collisional diffusion length (or skin depth) and  $\lambda_t$  is the spatial scale length over which the temperature modulation occurs. To obtain coupling to an Alfvén wave one expects that  $\lambda_t \sim 2\pi/k_A = 2\pi v_A/\omega$ ; this implies that the space charge term contributes a correction of order  $(m/M)(\omega v_e/\omega_{ci})^2$ . In the present study, parameters are chosen so that this correction plays a negligible role. The thermo-electric modulation arising from the  $\Delta T_e$  term in Eq. (3) is present even when  $E_0 = 0$ , i.e., in the absence of field aligned currents. This term can also contribute to the radiation of Alfvén waves due to both the parallel and perpendicular components of the gradient. The parallel contribution becomes relatively small for  $E_0 \gg T_e/e\lambda_t$ , while the perpendicular contribution ceases to dominate for  $E_0 \gg (\omega_{ci}/\omega)T_e/e\lambda_t$ . The amplitude of  $E_0$  is limited, however, because in order for the steady-state ohmic description to be applicable, the value of  $E_0$  must be smaller than the Dreicer runaway field. These constraints imply that in order for the field aligned currents to play a significant role in the radiation of Alfvén waves the following inequalities

$$\lambda_c^{-1} \gg (eE_0/T_e) \gg \lambda_t^{-1} \quad (4)$$

must be satisfied. In Eq. (4)  $\lambda_c = \bar{v}/v_e$  is the collisional mean free path for electrons, which of course, must satisfy  $\lambda_c \ll \lambda_t \sim v_A/\omega$  and  $\bar{v}$  is the electron

thermal velocity. In the present study we assume that the system under consideration satisfies Eq. (4) since otherwise the effect of field aligned currents would be masked by modulations accompanying the thermo-electric fields.

Next we proceed to determine the electric field  $\underline{E}$ . We Fourier analyse in configuration space and obtain

$$\tilde{\underline{E}}(\underline{k}) = \int_{-\infty}^{\infty} dx \int_{-\infty}^{\infty} dy \int_{-\infty}^{\infty} dz \exp[-i(k_x x + k_y y + k_z z)] \underline{E}(\underline{r}) . \quad (5)$$

Maxwell's wave equation yields

$$\underline{k} \times \underline{k} \times \tilde{\underline{E}} = -k_0^2 (\tilde{\underline{E}} - \frac{4\pi}{i\omega} \tilde{\underline{J}}) , \quad (6)$$

where  $\tilde{\underline{J}}$  is the Fourier transform of  $\underline{J}$ , and  $k_0 = \omega/c$ . From Eq.(3a), the Fourier transformed current of Eq.(6) may be written as

$$\tilde{\underline{J}} = \tilde{\sigma}(\omega) \cdot \tilde{\underline{E}} + \hat{z} \sigma_{z0} AF(k_x, k_y, k_z) , A = \left( \frac{\Delta \sigma_z}{\sigma_{z0}} \right)_m E_0 , \quad (7)$$

where  $F$  is the Fourier transform of  $f(x, y, z)$ , and where we have assumed that the parallel ac conductivity  $\sigma_z \approx \sigma_{z0}$ , the unperturbed dc value. This assumption is correct for the frequency range specified in Eq.(1).

We solve Eq.(6) for the unknown field  $\tilde{\underline{E}}$  and obtain

$$\tilde{E}_{x,y} = \frac{k_z g_{x,y}}{D(\underline{k}, \omega)} \left( \frac{1}{\epsilon_{||}} - 1 \right) AF \quad (8)$$

with the notation  $\tilde{E}_{x,y}$  meaning either  $\tilde{E}_x$  or  $\tilde{E}_y$  and likewise for other variables. In Eq. (8) the coupling factor is

$$g_{x,y} = k_{x,y} (k^2 - k_0^2 \epsilon_{\perp}) \pm k_{y,x} k_0^2 \epsilon_{xy} , \quad (9)$$

with the (+) sign for  $g_x$  and the (-) sign for  $g_y$ . In here  $\epsilon_{\perp}$  is the perpendicular component of the dielectric tensor for a cold collisional plasma and  $\epsilon_{xy}$  the corresponding off-diagonal component, the parallel component is  $\epsilon_{\parallel}$ . The denominator in Eq. (8) leads to the dispersion relation containing both the shear and compressional Alfvén modes and is more clearly expressed in the form

$$D(\underline{k}, \omega) = (k_z^2 - k_s^2) (k_z^2 - k_c^2) , \quad (10)$$

with

$$k_{s,c}^2 = k_0^2 \epsilon_{\perp} \pm (1/2) \{ [k_{\perp}^4 (1 - \epsilon_{\perp}/\epsilon_{\parallel})^2 + 4k_0^4 \epsilon_{xy} \epsilon_{yx} (1 - k_{\perp}^2/k_0^2 \epsilon_{\parallel})]^{1/2} \\ \mp k_{\perp}^2 (1 + \epsilon_{\perp}/\epsilon_{\parallel}) \} , \quad (11)$$

where the upper sign goes with  $k_s^2$  and the lower sign with  $k_c^2$ . Physically, the  $k_s$  and  $k_c$  roots correspond to the parallel wave number of the shear and compressional modes, respectively, for fixed values of  $k_{\perp} = (k_x^2 + k_y^2)^{1/2}$  and  $\omega$ . For the sake of clarity the characteristic topology of these roots for a fixed value of  $\omega < \omega_{ci}$  is shown in Fig. 2 as a function of  $k_{\perp}^2$ . As is well known, the shear mode is essentially insensitive to variations in  $k_{\perp}$ , while the compressional mode exhibits an abrupt cut-off for a  $k_{\perp}$  slightly below  $k_A$ . The topology of these roots plays an important role in the evaluation of the radiation pattern associated with the hot spot. It should be noted that in the limit  $\omega/\omega_{ci} \ll 1$ ,  $k_s^2 \approx k_A^2 (1 + i\nu_i/\omega)$  and  $k_c^2 \approx k_A^2 (1 + i\nu_i/\omega) - k_{\perp}^2$ .

Because of the high electron conductivity along the magnetic field,  $\epsilon_{\parallel}$  is a large quantity having negligible contribution on low frequency waves as may be clearly seen in Eqs. (8) and (11) when we let  $\epsilon_{\parallel} \rightarrow \infty$ . However, it is kept in the analysis for the sake of completeness. The large  $\epsilon_{\parallel}$  approximation is also used in calculating the  $z$  component of the electric field, which is obtained either in  $\underline{k}$  space from Eqs. (6) and (7) as

$$\tilde{E}_z \approx -AF(k_x, k_y, k_z) , \quad (12)$$

or in configuration space from the  $z$  component of Eq.(3a)

$$E_z \approx -\left(\frac{\Delta\sigma_z(x, y, z)}{\sigma_{z0}}\right)E_0 , \quad (12a)$$

where the contribution from  $J_z/\sigma_{z0}$  is negligibly small. Current modulation parallel to the magnetic field is therefore negligible, with  $E_z$  keeping the initial current  $J_0 \hat{z}$  nearly constant. The transverse variation of  $E_z$  implies that transverse electric fields are generated and associated polarization currents are forced to flow in the region where the hot spot is formed. These locally forced currents create a self-consistent field in the neighborhood of the hot spot which appears in the analysis in the form of a near field. In addition, outwardly propagating Alfvén waves emanate from the locally forced currents; these waves have quasi-transverse electric fields with  $E_z$  negligibly small outside the hot spot.

Next we proceed to invert the Fourier transformed field  $\tilde{E}$  to obtain the radiation pattern in configuration space. Since the source has azimuthal symmetry, it is advantageous to use a cylindrical coordinate system in  $\underline{k}$  space as well as in configuration space to obtain

$$E_{x,y}(\rho, \phi, z) = \frac{-A}{(2\pi)^3} \int_0^\infty dk_\perp k_\perp \int_{-\infty}^\infty dk_z \int_0^{2\pi} d\alpha \frac{k_z g_{x,y}(k_\perp, k_z, \alpha)}{(k_z^2 - k_s^2)(k_z^2 - k_c^2)} F(k_\perp, k_z) \exp\{i[k_z z + k_\perp \rho \cos(\alpha - \phi)]\} \quad , \quad (13)$$

where  $(\rho, \phi)$  are the radial and azimuthal coordinates in configuration space and  $(k_\perp, \alpha)$  are the conjugate quantities in k space.

It should be noted that in the integrand of Eq. (13) the only  $\alpha$  dependence, aside from the expected exponential factor, arises through  $g_{x,y}$  and that such a dependence, as seen from Eq. (9), is proportional to either  $\sin\alpha$  or  $\cos\alpha$ . This implies that the required integrations over  $\alpha$  are of the form

$$\int_0^{2\pi} d\alpha (\sin\alpha, \cos\alpha) \exp[i k_\perp \rho \cos(\alpha - \phi)] = 2\pi i J_1(k_\perp \rho) (\sin \phi, \cos \phi), \quad (14)$$

where  $J_1$  is the first order Bessel function.

Expressing the electric field components in cylindrical coordinates through the relation  $E_x = E_\rho \cos\phi - E_\phi \sin\phi$ ,  $E_y = E_\rho \sin\phi + E_\phi \cos\phi$  and using Eq. (14) yields,

$$E_{\rho, \phi}(\rho, \phi, z) = \frac{-iA}{(2\pi)^2} \int_0^\infty dk_\perp k_\perp^2 \int_{-\infty}^\infty dk_z \left[ \frac{F(k_\perp, k_z) J_1(k_\perp \rho) e^{ik_z z}}{(k_z^2 - k_s^2)(k_z^2 - k_c^2)} \right] h_{\rho, \phi}, \quad (15)$$

where again, the factor  $h_\rho = (k_\perp^2 + k_z^2 - k_0^2 \epsilon_\perp)$  goes with  $E_\rho$  and  $h_\phi = (-k_0^2 \epsilon_{xy})$  with  $E_\phi$ , and

$$F(k_\perp, k_z) = (\pi)^3/2 (d_\parallel d_\perp^2) \exp\{-\frac{1}{4} [k_\perp^2 d_\perp^2 + k_z^2 d_\parallel^2]\}. \quad (16)$$

Next we proceed to perform the  $k_z$  integration by making a suitable distortion of the contour of integration in the complex  $k_z$  plane. For  $z > 0$  the relevant features of the integrand are the existence of two simple poles at  $k_s$  and  $k_c$  with  $\text{Im} \{k_s, k_c\} > 0$ , and a saddle point at  $k_{sp} = i2z/d_{\parallel}^2$ , as is indicated in Fig. 3. It is evident from Eq. (11) that the location of the poles is a function of  $k_{\perp}$ , which is also shown in Fig. 3. For  $k_{\perp} \rightarrow 0$  the two poles are close to each other, and as  $k_{\perp}$  increases the  $k_c$  pole goes to infinity along a line parallel to the imaginary axis. The  $k_s$  pole, however, remains essentially fixed as  $k_{\perp}$  varies. The saddle point is independent of  $k_{\perp}$  and its noteworthy feature is that for some value of  $k_{\perp}$  the  $k_c$  pole may be close to it. Such a behavior can be handled by applying a technique prescribed by Banos<sup>2</sup> and outlined in Appendix A. Since the hot spot is symmetric in  $z$ , analogous features in the lower part of the complex  $k_z$  plane are relevant for  $z < 0$ , and need no additional consideration.

The technique used for evaluating the  $k_z$  integration consists in deforming the initial contour  $C$  to the new contour  $C'$  shown in Fig. 3. Contour  $C'$  begins at  $\text{Re } k_z \rightarrow -\infty$  and is forced to pass through the saddle point at  $i2z/d_{\parallel}^2$ . The contour passes below the  $k_c$  pole (pole to the left of contour) and finally goes to  $\text{Re } k_z \rightarrow \infty$  by passing above the  $k_s$  pole (pole to the right of contour). The first step in evaluating the  $k_z$  integral (defined by  $I$ ) consists of separating the individual contributions of each pole by writing the integrand in terms of partial fractions, i.e.,

$$(k_z^2 - k_s^2)^{-1} (k_z^2 - k_c^2)^{-1} = (k_s^2 - k_c^2)^{-1} [(k_z^2 - k_s^2)^{-1} - (k_z^2 - k_c^2)^{-1}].$$

The desired integral is then  $I = I_s + I_c$ , where  $I_s$  is the integral having the pole at  $k_s$  and  $I_c$  is the integral having the pole  $k_c$ .

The  $I_s$  integral can be readily evaluated because the pole at  $k_s$  remains far from the saddle point for all values of  $k_{\perp}$ . Consequently, the influence

of the pole on the evaluation of the saddle point contribution is negligible for this case. Using Cauchy's theorem and approximating the path contribution along  $C'$  by the standard saddle point value  $I_{sp}$  results in

$$I_s = I_{sp} + 2\pi i \text{ Residue } (k_z = k_s). \quad (17)$$

The evaluation of  $I_c$  using the  $C'$  contour requires proper attention to the possibility that the pole at  $k_c$  may be found close to the saddle point. However, we may write the result symbolically in the form

$$I_c = I'_{sp} + 2\pi i \text{ Residue } (k_z = k_c), \quad (18)$$

where now  $I'_{sp}$  represents the saddle point result properly corrected for the presence of the pole. The details leading to the evaluation of  $I_c$  are given in Appendix A; it suffices to mention here that the result involves the familiar plasma dispersion function evaluated at a parameter  $\zeta = k_c d_{\parallel}/2 - iz/d_{\parallel}$ .

Combining the details involved in evaluating the expressions in Eqs. (17) and (18) transforms Eq. (15) into the following well behaved integral:

$$E_{\rho, \phi}(\rho, z) = \frac{-A}{4} d_{\parallel} d_{\perp}^2 \int_0^{\infty} \frac{dk_{\perp} k_{\perp}^2 J_1(k_{\perp} \rho)}{[k_{\perp}^4 (1 - \epsilon_{\perp}/\epsilon_{\parallel})^2 + 4k_0^4 \epsilon_{xy} \epsilon_{yx} (1 - k_{\perp}^2/k_0^2 \epsilon_{\parallel})]^{1/2}} \exp(-k_{\perp}^2 d_{\perp}^2/4) [G_{\rho, \phi} + K_{\rho, \phi} + Q_{\rho, \phi}] \quad , \quad (19)$$

$$G_{\rho, \phi} = i\sqrt{\pi} \exp(-k_s^2 d_{\parallel}^2/4 + ik_s z) h_{\rho, \phi} (k_z = k_s) \quad , \quad (20)$$

$$K_{\rho, \phi} = -(1/2) \exp(-z^2/d_{\parallel}^2) h_{\rho, \phi} (k_z = k_c) z(\zeta) \quad , \quad (21)$$

$$Q_{\rho, \phi} = -\exp(-z^2/d_{\parallel}^2) \left\{ \delta_{\rho, \phi} (k_c d_{\parallel} + i2z/d_{\parallel})/d_{\parallel}^2 \right. \\ \left. + (1/2) h_{\rho, \phi} (k_z = i2z/d_{\parallel}^2) [(i2z/d_{\parallel})(z^2/d_{\parallel}^2 + k_s^2 d_{\parallel}^2/4)^{-1} \right. \\ \left. + (k_c d_{\parallel}/2 + iz/d_{\parallel})^{-1}] \right\} \quad (22)$$

where  $\delta_{\rho} = 1$ ,  $\delta_{\phi} = 0$ ,  $\zeta = k_c d_{\parallel}/2 - iz/d_{\parallel}$ , and

$$Z(\zeta) = \frac{1}{\sqrt{\pi}} \int_{-\infty}^{\infty} dt \frac{e^{-t^2}}{t - \zeta} + i\sigma \sqrt{\pi} e^{-\zeta^2}, \quad (23)$$

$$\sigma = \begin{cases} 0 & \text{Im } \zeta > 0 \\ 1 & \text{Im } \zeta = 0 \\ 2 & \text{Im } \zeta < 0 \end{cases} \quad (24)$$

is the plasma dispersion function. When  $\sigma = 1$  (for  $\text{Im } \zeta = 0$ ) in Eq.(24), the integral in Eq.(23) is to be interpreted as Cauchy's principal value integral.

Physically, the terms contained in  $G_{\rho, \phi}$  represent the fields associated with the shear Alfvén mode. For  $\omega/\omega_{ci} \ll 1$  this term is the dominant contribution to the radiation pattern. The radial dependence of the shear Alfvén mode is primarily determined by the factor  $k_{\perp}^2 J_1(k_{\perp} \rho) \exp(-k_{\perp}^2 d_{\perp}^2/4)$  in the integrand; it shows that the shear mode fields vanish at  $\rho = 0$  and peak at some fraction of  $d_{\perp}$ , i.e., they create a ring-like pattern highly collimated along the flux tube passing through the hot spot. The  $K_{\rho, \phi}$  term contains the contribution of the compressional mode, which for  $\omega < \omega_{ci}$  is much smaller than the shear mode. The fact that a portion of the spectrum with  $k_{\perp} > k_A$  does not contribute to a propagating mode (Fig. 2) is properly taken care of by the  $Z$  function in the  $K_{\rho, \phi}$  term. The weak excitation of the compressional mode is evident from the coupling coefficient  $h_{\rho}$  of Eq (15). Finally, the  $Q_{\rho, \phi}$  term

term contains purely near field effects associated with the local conductivity modulation.

### III. Radiation Pattern

To obtain detailed quantitative information about the spatial variation of the electric fields produced by the conductivity modulation, the  $k_{\perp}$  integration in Eq. (19) is performed numerically for specific parameter values.

Figure 4 shows the radial profile of the magnitude of each of the electric field components, scaled to  $|A| = (\Delta\sigma_z/\sigma_{z0})_m E_0$ , for different axial positions. The parameters used are  $c/v_A = 390$ ,  $\omega/\omega_{ci} = 0.23$ ,  $v_{\perp}/\omega = 2 \times 10^{-4}$ ,  $k_A d_{\parallel} = k_A d_{\perp} = 1$ . Figure 4a shows the radial field  $E_{\rho}$  which is dominated at large  $z$  by the contributions due to the shear mode. The characteristic headlight pattern with null field on axis, common to other field aligned excitation scenarios,<sup>3</sup> exhibits a peak at  $k_A \rho \sim 0.7$  and decays rapidly for  $k_A \rho > 2$  (i.e., it behaves as  $\exp(-\rho^2/d_{\perp}^2)$ ). Figure 4b displays the azimuthal field  $E_{\phi}$  which is much smaller than  $E_{\rho}$  (note factor of 10 in scale). In addition to the headlight pattern associated with the shear mode contribution,  $E_{\phi}$  exhibits a small, but slowly decaying, feature at large  $\rho$  corresponding to the radiated compressional mode.

The axial dependence of  $E_{\rho}$  and  $E_{\phi}$  is shown in Fig. 5 for a fixed radial position near the peak of the headlight pattern, i.e.,  $k_A \rho = 0.7$ . It is evident from the presentation that within  $k_A z \sim 1.5$  the shear mode attains its asymptotic value with a polarization  $|E_{\rho}| \gg |E_{\phi}|$ .

The individual contributions to the total  $E_{\rho}$  (i.e., arising from the  $G_{\rho}$ ,  $K_{\rho}$ , and  $Q_{\rho}$  terms in Eq. (19)) are shown in Fig. 6 as a function of radius for different axial positions. In Fig. 6a one observes that the shear mode contribution is essentially constant beyond  $k_A z = 0.5$ . This behavior is to be contrasted with Fig. 5, where it is seen that the total  $E_{\rho}$  does not reach its

asymptotic value until  $k_A z \approx 1.5$ . The difference between these two figures is attributable to the contributions arising from the near field, shown in Fig. 6c. For  $k_A z < 1$  the near field contribution tends to cancel the pure shear mode contribution and results in the net pattern shown in Figs. 4 and 5. The radially spreading nature of the compressional mode is visible in Fig. 6b where it is clear that at large axial values  $k_A z = 2.5$  the peak moves further away from the magnetic flux tube formed by the shear mode of Fig. 6a.

The previously discussed field patterns pertain to a spherically symmetric hot spot, i.e.,  $d_{\parallel} = d_{\perp}$ . The effect of changing  $d_{\parallel}/d_{\perp}$  on  $E_{\rho}$  is shown in Fig. 7 for a cigar-like spot, i.e., longer along the field line than across it ( $k_A d_{\perp} = 0.5$ ,  $k_A d_{\parallel} = 1$ ), a spherical spot ( $k_A d_{\perp} = 1$ ,  $k_A d_{\parallel} = 1$ ), and a pancake-like spot, i.e., larger perpendicular to the field than along it ( $k_A d_{\perp} = 1$ ,  $k_A d_{\parallel} = 0.5$ ). Fig. 7 illustrates that the headlight pattern due to the shear mode becomes narrower and of larger intensity for the cigar-like spot than for the spherical one. For the pancake-like spot the headlight pattern is similar to that obtained for the spherical spot, but the magnitude of the electric field is reduced.

Another quantity of interest is the time averaged Poynting vector  $\underline{S} = (c/8\pi) \operatorname{Re} (\underline{E} \times \underline{B}^*)$ , which in the present problem has a natural scaling factor  $S_0 \equiv (c^2/v_A) |A|^2/8\pi$ . The radial dependence of the various components of  $\underline{S}$  is shown in Fig. 8 for selected values of  $z$ , and for the same conditions leading to Figs. 4-6. It is clear from Figs. 8a and 8b that at these low frequencies power is radiated predominantly along the confining magnetic field ( $z$  direction) with a highly collimated headlight pattern passing through the hot spot. A much smaller fraction of the total radiated power is carried away by the compressional mode out in the direction perpendicular to the magnetic field. In addition, there is a circulating Poynting vector component in the azimuthal direction  $S_{\phi}$ , shown in Fig. 8c. This circulating component does not lead to net radiation.

Finally, it is useful to introduce a scaled figure of merit, that characterises the radiation efficiency of this system. Of the possible scaling factors that can be considered, perhaps the more meaningful is the amount of power going into the ohmic modulation at frequency  $\omega$ , i.e., the volume integral of  $\Delta\sigma_z E_0^2/2$ . Using this definition leads to

$$\eta = \frac{\iint \underline{S} \cdot \underline{da}}{\iint \iint \frac{1}{2} \Delta\sigma_z E_0^2 dv} , \quad (25)$$

$$\eta = \frac{1}{4\pi} \left(\frac{c}{v_A}\right)^2 \left(\frac{\Delta\sigma_z}{\sigma_{zo}}\right)_m \left(\frac{\omega}{\sigma_{zo}}\right) \bar{\eta} , \quad (26)$$

where  $\bar{\eta}$  is a scaled geometric factor that must be evaluated for a particular shape of the hot spot. The order of magnitude of  $\bar{\eta}$  is  $S_z/S$ . The important parameter dependences, however, are contained in the factor multiplying  $\bar{\eta}$  in Eq. (26). The enhancement due to  $v_A$  shows up in the form  $(c/v_A)^2$ , and the expected low inefficiency inherent to all low frequency schemes is measured by  $(\omega/\sigma_{zo})$ . Since the process considered is linear, the dependence on  $(\Delta\sigma_z/\sigma_{zo})_m$ , i.e., the depth of modulation, enters linearly. Equation (26) may also be expressed as  $\eta = (\omega/\omega_{ci})(v_e/\omega_{ce})(\Delta\sigma_z/\sigma_{zo})\bar{\eta}$ , which is another way of looking at the parameter dependence of the efficiency, and showing that it is density independent.

#### IV. Conclusions

The radiation pattern generated by a field aligned current due to a localized modulation of the electrical conductivity at a frequency  $\omega$  below the ion cyclotron frequency  $\omega_{ci}$  has been calculated. The pattern consists of a

shear Alfvén mode, a compressional Alfvén mode, and near fields. The shear mode propagates in a highly collimated pattern along the magnetic field lines passing through the hot spot giving rise to the modulation, while the compressional mode is emitted over a broad range of angles and moves radially away from the hot spot. For  $\omega/\omega_{ci} < 1$ , nearly 90% of the radiated power appears in the form of the shear mode with the remaining 10% being taken away by the compressional mode.

The radiation efficiency for this system is found to scale according to  $(c/v_A)^2 (\omega/\sigma_{z0}) (\Delta\sigma_z/\sigma_{z0})$ , thus indicating the enhancement associated with the high index of refraction found in a magnetized plasma. However, the inherent inefficiency associated with the generation of low-frequency electric fields in a highly conducting plasma mitigates the enhancement by the factor  $\omega/\sigma_{z0}$ . For parameters characteristic of the auroral ionosphere, where naturally occurring field aligned currents are present,<sup>1,4</sup> it is found that  $n \sim 10^{-5}$  and the magnitude of the transverse electric fields associated with the shear mode can be comparable to the magnitude  $E_0$  of the field driving the current system. Although this low frequency generation scheme appears inefficient for practical usage, because the shear mode is highly collimated, it may be possible for properly placed detectors to sample this component.<sup>5</sup>

It is worth noting that although we have been primarily motivated to consider the modulation of field aligned currents arising due to an external electron heating source, the ideas presented here and the techniques for calculating the fields, described in Sec. II, can be applied to situations in which field aligned modulations arise by other means. For instance, in a recent experiment in a research tokamak Borg, et.al.<sup>6</sup> have modulated the current in a field aligned external wire. Preliminary measurements have shown the generation of a shear mode having a headlight pattern similar to the type discussed in this paper. It is also found by these experimentalists that the radiated

compressional mode is much weaker than the shear mode. Another situation in which related phenomena occur, albeit without direct external control, is in the appearance of the well known sawtooth oscillations attributed to temperature relaxations in tokamaks.<sup>7</sup>

ACKNOWLEDGEMENTS

The authors thank Prof. A. Baños, Jr. for illuminating discussions concerning saddle point integration methods.

This work is supported by the Office of Naval Research.

Appendix A

The integral of Eq. (18)

$$I_c = I'_{sp} + 2\pi i \text{ Residue } (k_z = k_c) \quad (A1)$$

contains a saddle point integration  $I'_{sp}$  where the analyticity condition imposed on the integrand is affected by the presence of a first order pole at  $k_z = k_c$  that is in the neighborhood of the saddle point at  $k_z = k_{sp}$ . Following the treatment of Baños,<sup>2</sup> this situation is properly handled by expressing the saddle point integration as

$$I'_{sp} = I_a + I_p, \quad (A2)$$

where we have separated the regular analytic part of the integral  $I_a$  from the part containing the effect of the pole  $I_p$ .

From Eqs. (13)-(18), we write the integrand of Eq. (A1) as

$$\Phi(k_z) = \frac{k_z g(k_z)}{k_z^2 - k_c^2} \exp(-k_z^2 d_1^2/4 + ik_z z), \quad (A3)$$

where  $g(k_z)$  is an analytic function in the complex  $k_z$  plane. Using partial fractions Eq. (A3) is rewritten as

$$\Phi(k_z) = \frac{1}{2} \left( \frac{1}{k_z + k_c} + \frac{1}{k_z - k_c} \right) g(k_z) \exp(-k_z^2 d_1^2/4 + ik_z z) = \Phi_- + \Phi_+. \quad (A4)$$

The first term of Eq. (A4),  $\Phi_-$ , has a pole at  $k_z = -k_c$  away from the saddle point (for positive  $z$  (Fig. 3)). Therefore, its contribution to the saddle point integration is calculated in the usual manner. The second term  $\Phi_+$  with the pole at  $k_z = k_c$  passing in the vicinity of the saddle point is properly

handled by expanding the analytic function  $g(k_z)$  about  $k_c$ , which yields

$$\Phi_+(k_z) = \frac{1}{2} \left[ \frac{g(k_c)}{k_z - k_c} + g'(k_c) + \frac{g''(k_c)(k_z - k_c)}{2!} + \dots \right] \exp(-k_z^2 d_{\parallel}^2/4 + ik_z z), \quad (A5)$$

where the primes denote derivatives with respect to  $k_z$ .

From Eqs. (A2), (A4), and (A5) we can write the integrand of  $I_a$  as

$$\Phi_a(k_z) = \frac{1}{2} \left[ \frac{g(k_z)}{k_z + k_c} + g'(k_c) + \frac{g''(k_c)}{2!} (k_z - k_c) + \dots \right] \exp(-k_z^2 d_{\parallel}^2/4 + ik_z z), \quad (A6)$$

and the integrand of  $I_p$  as

$$\Phi_p(k_z) = \frac{1}{2} \frac{g(k_c)}{k_z - k_c} \exp(-k_z^2 d_{\parallel}^2/4 + ik_z z). \quad (A7)$$

The task of evaluating  $I_c$  along the contour  $C'$  of Fig. 3 is now greatly facilitated by rewriting Eq.(A1) as

$$I_c = I_a + I_b = I_a + [I_p + 2\pi i \text{ Residue } (k_z = k_c)] \quad (A8)$$

From Eq. (A6) it is clear that the integral  $I_a$  is easily evaluated along the contour  $C'$  using the common saddle point method, while the term in square brackets in Eq. (A8) containing the effect of the pole is written as

$$\begin{aligned} I_b &= I_p + 2\pi i \text{ Residue } (k_z = k_c) \\ &= \frac{\sqrt{\pi}}{2} g(k_c) \exp(-z^2/d_{\parallel}^2) Z(\zeta), \end{aligned} \quad (A9)$$

where  $\zeta = (k_c d_{\parallel}/2 - iz/d_{\parallel})$  and  $Z(\zeta)$  is the plasma dispersion function defined in Eqs. (23) and (24).

When  $k_c$ , which is a function of  $k_\perp$  (Fig. 3), is away from  $k_{sp}$ , the value of  $Z(\zeta)$  is such that the pole has negligible contribution to the saddle point integration. As  $k_c$  gets closer to  $k_{sp}$ ,  $Z(\zeta)$  takes values that properly account for the presence of the pole near  $k_{sp}$ . This result is valid for all values of  $\zeta$  in the complex  $k_z$  plane.

Bibliography

1. Merit Shoucri, G.J. Morales, and J.E. Maggs, *J. Geophys. Res.*, 89, 2907 (1984).
2. A. Baños, Jr., Dipole radiation in the presence of a conducting half-space (Pergamon Press, New York, 1966), p. 71.
3. Merit Shoucri, G.J. Morales, and J.E. Maggs, *Phys. Fluids*, 25, 1824 (1982).
4. P.F. Bythrow, *J. Geophys. Res.*, to be published.
5. H.G. James, R.L. Dowden, M.T. Rietveld, P. Stubbe, and H. Kopka, *J. Geophys. Res.*, 89, 1655 (1984).
6. C. Borg, M.H. Brennan, R.C. Cross, and L. Giannone, in Proceedings of the International Conference on Plasma Physics, Lausanne, Switzerland, 1984 (Ecole Polytechnique Federale de Lausanne, Switzerland, 1984). Vol. II, p. 230.
7. G. Jahns, M. Soler, B.V. Waddell, J.D. Callen, and H.R. Hicks, *Nucl. Fusion*, 18, 609 (1978).

Figure Captions

Fig. 1 Schematic representation of the model showing the collimated headlight pattern of the radiated shear Alfvén wave.

Fig. 2 Dispersion relation showing  $k_z^2$  versus  $k_{\perp}^2$  for fixed  $\omega/\omega_{ci} = 0.23$  and  $n_A = 390$ .

Fig. 3 Location of the poles and saddle points in the complex  $k_z$  plane for the  $k_z$  integral of Eqs. (17) and (18) (for  $z > 0$ ). The initial contour  $C$  is deformed to  $C'$ .

Fig. 4 Radial profile of the normalized magnitude of the (a) radial and (b) azimuthal electric field components at two axial positions  $k_A z = 0.5$  (near field) and  $k_A z = 2.5$  (far field),  $\omega/\omega_{ci} = 0.23$ ,  $n_A = 390$ ,  $k_A d_{\parallel} = k_A d_{\perp} = 1$ .

Fig. 5 Axial profile of the normalized magnitude of the electric field components  $E_{\rho}$  and  $E_{\phi}$  at a fixed radial position  $k_A \rho = 0.7$ . Same parameters as in Fig. 4. Constant magnitude at large axial distance is due to the shear Alfvén mode.

Fig. 6 Radial profiles of the components of  $E_{\rho}$  at the same axial locations shown in Fig. 4 for the same parameters: (a) shear Alfvén wave; (b) compressional Alfvén wave; (c) near fields.

Fig. 7 Dependence of  $E_{\rho}$  on the source size for  $\omega/\omega_{ci} = 0.23$  and  $n_A = 390$ . Heated volume is (a) cigar-like; (b) symmetric; (c) pancake-like.

Fig. 8 Normalized Poynting flux components for the fields of Fig. 4. Over 90% of the power is radiated in the  $z$  direction.

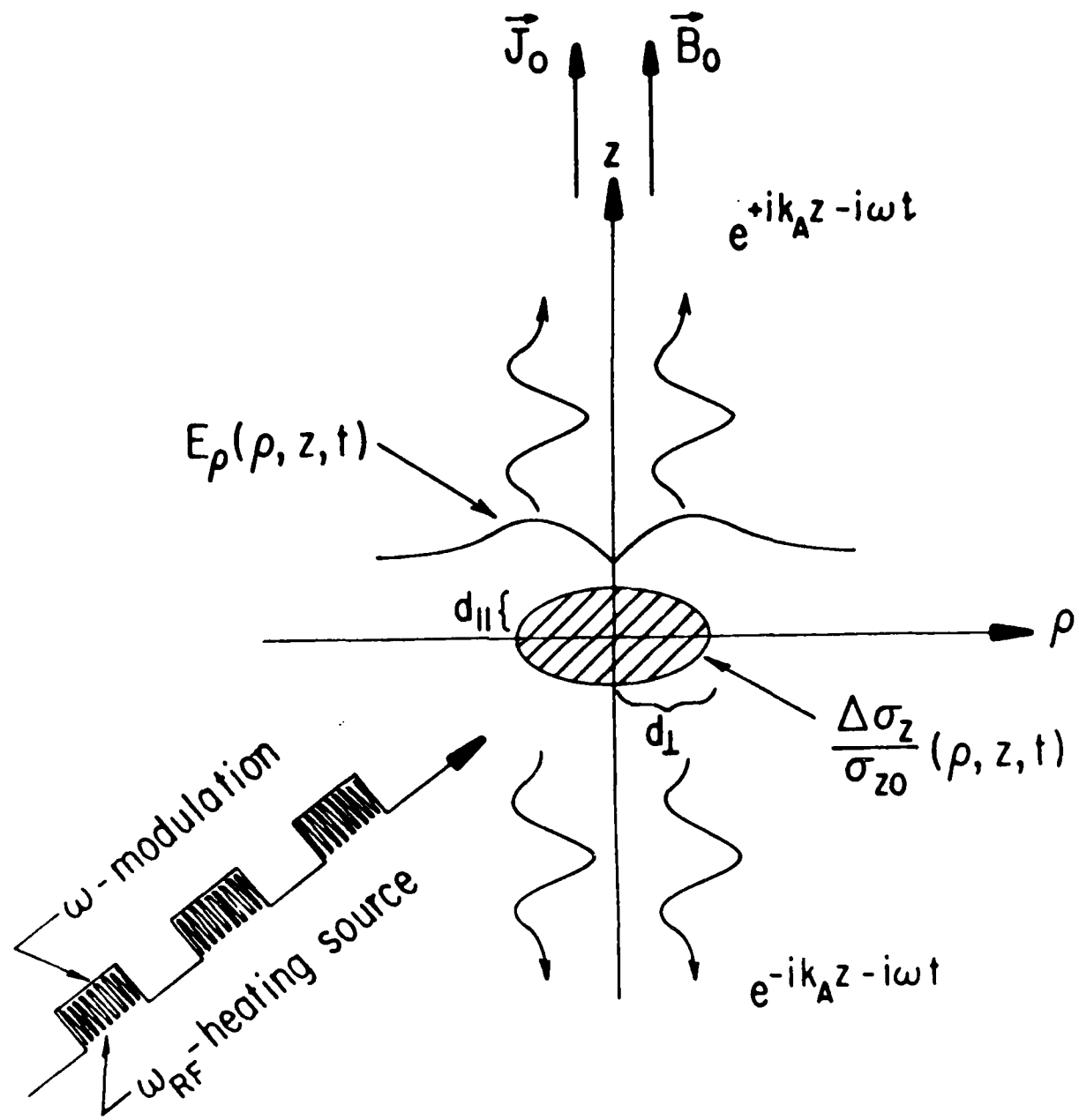


Fig. 1

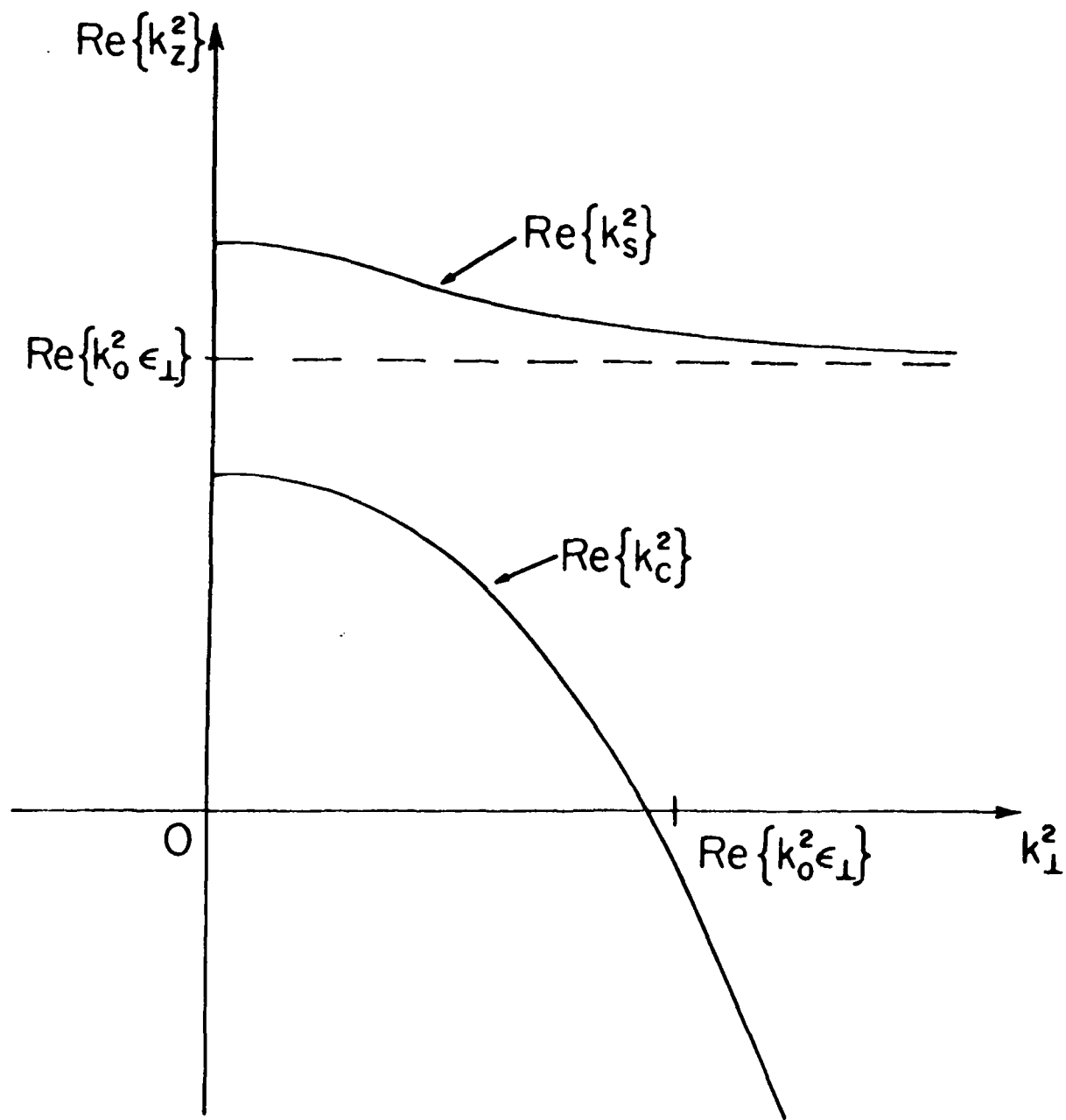
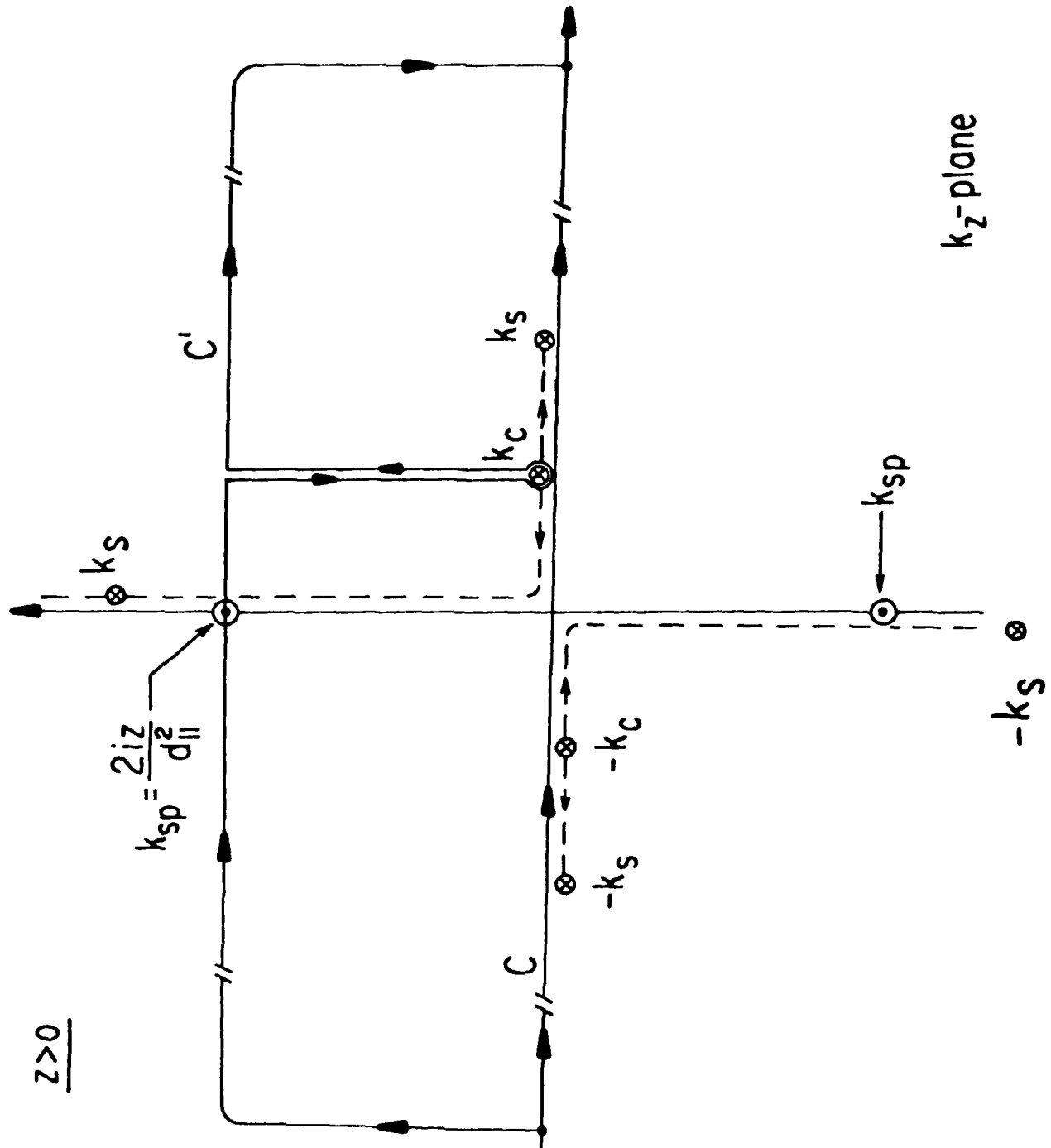


Fig. 2



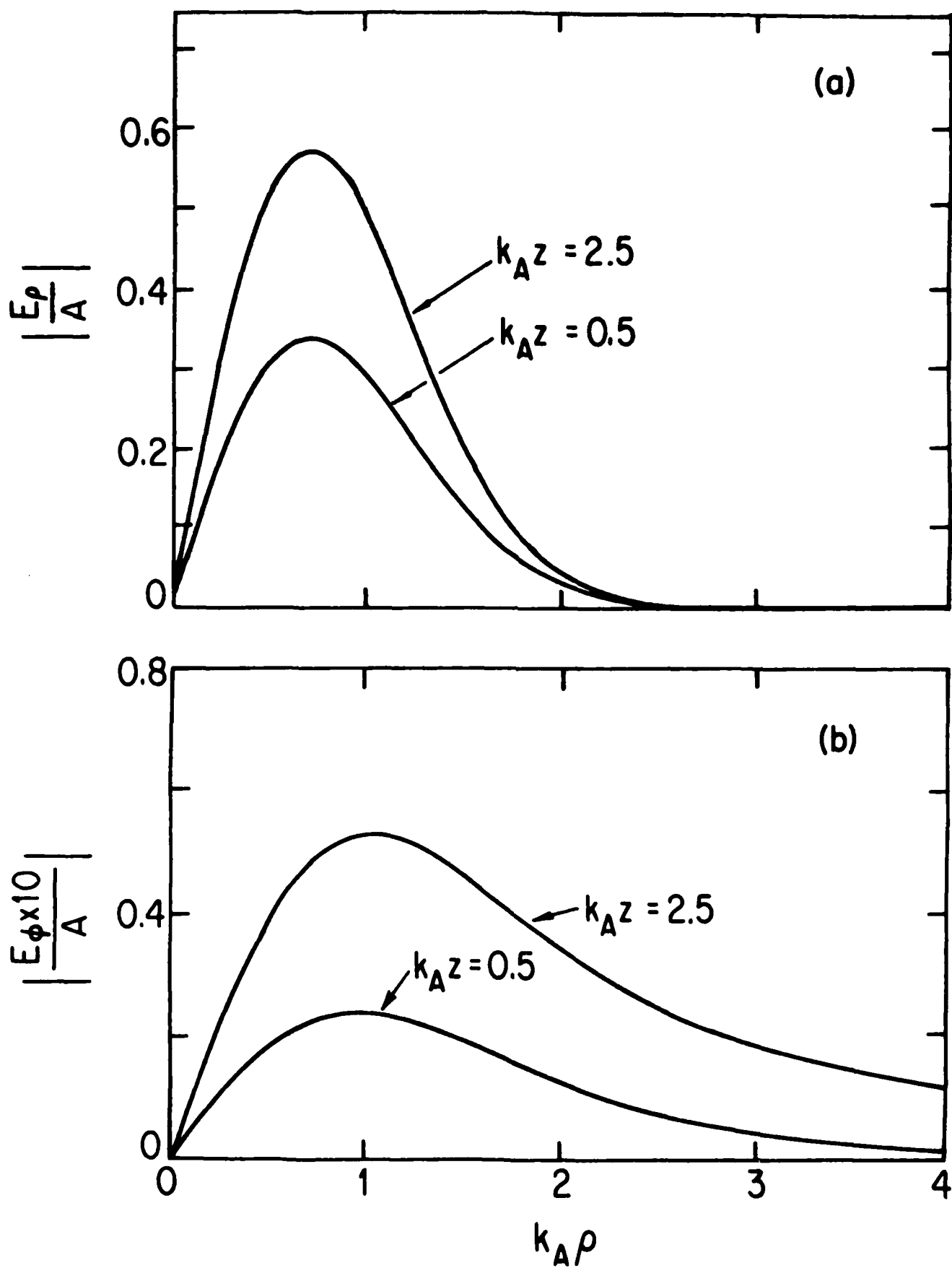


Fig. 4

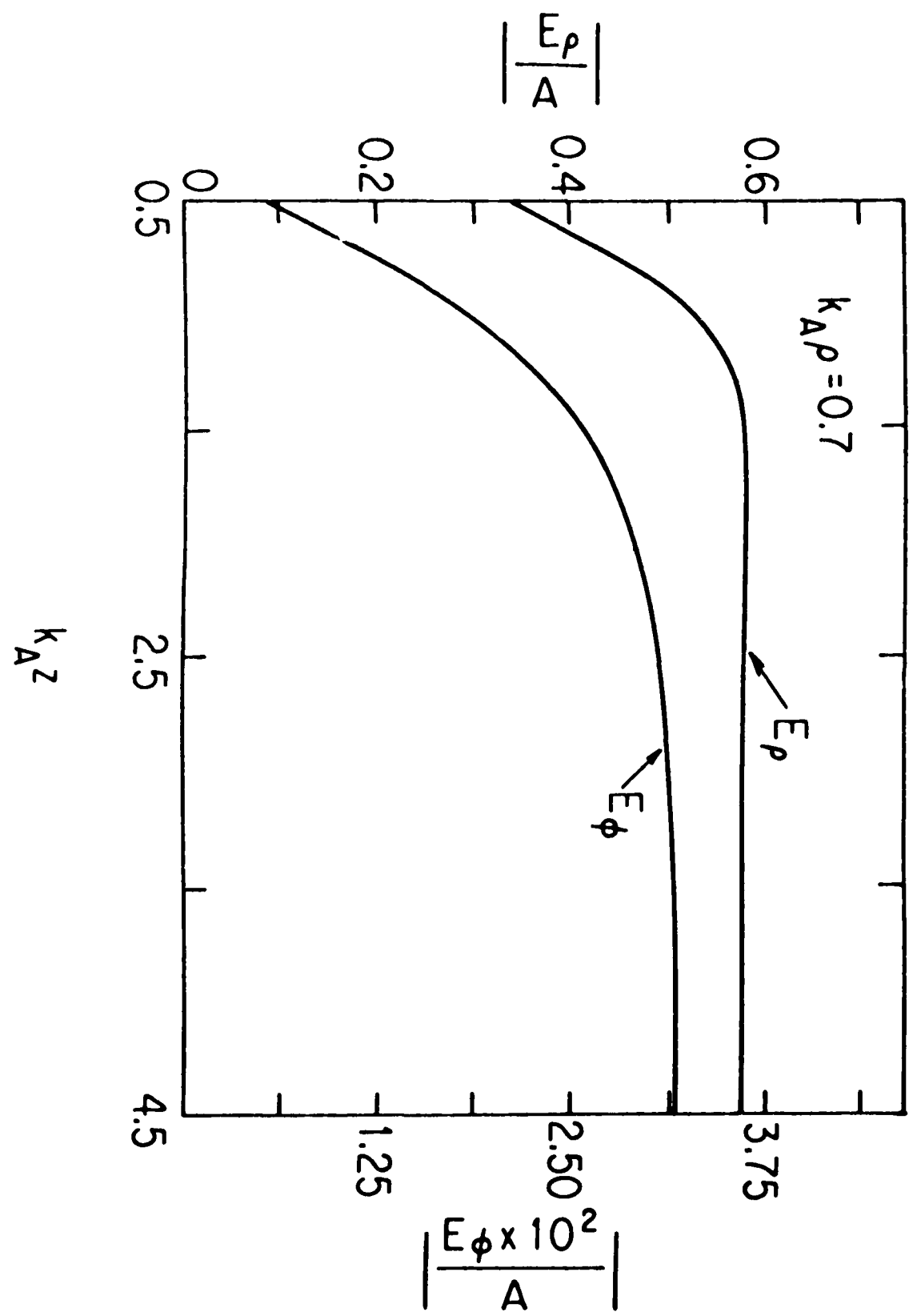


Fig. 5

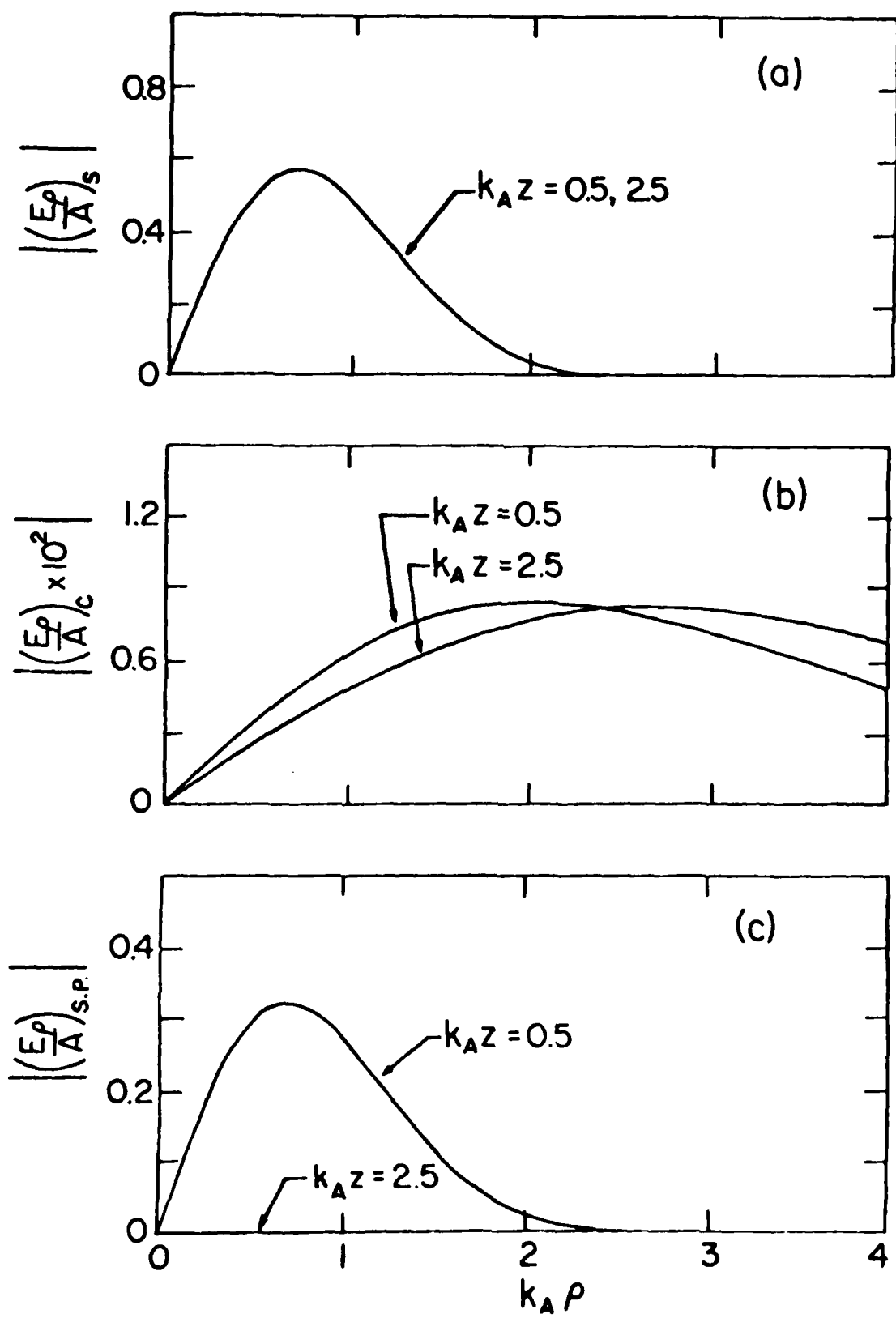


Fig. 6

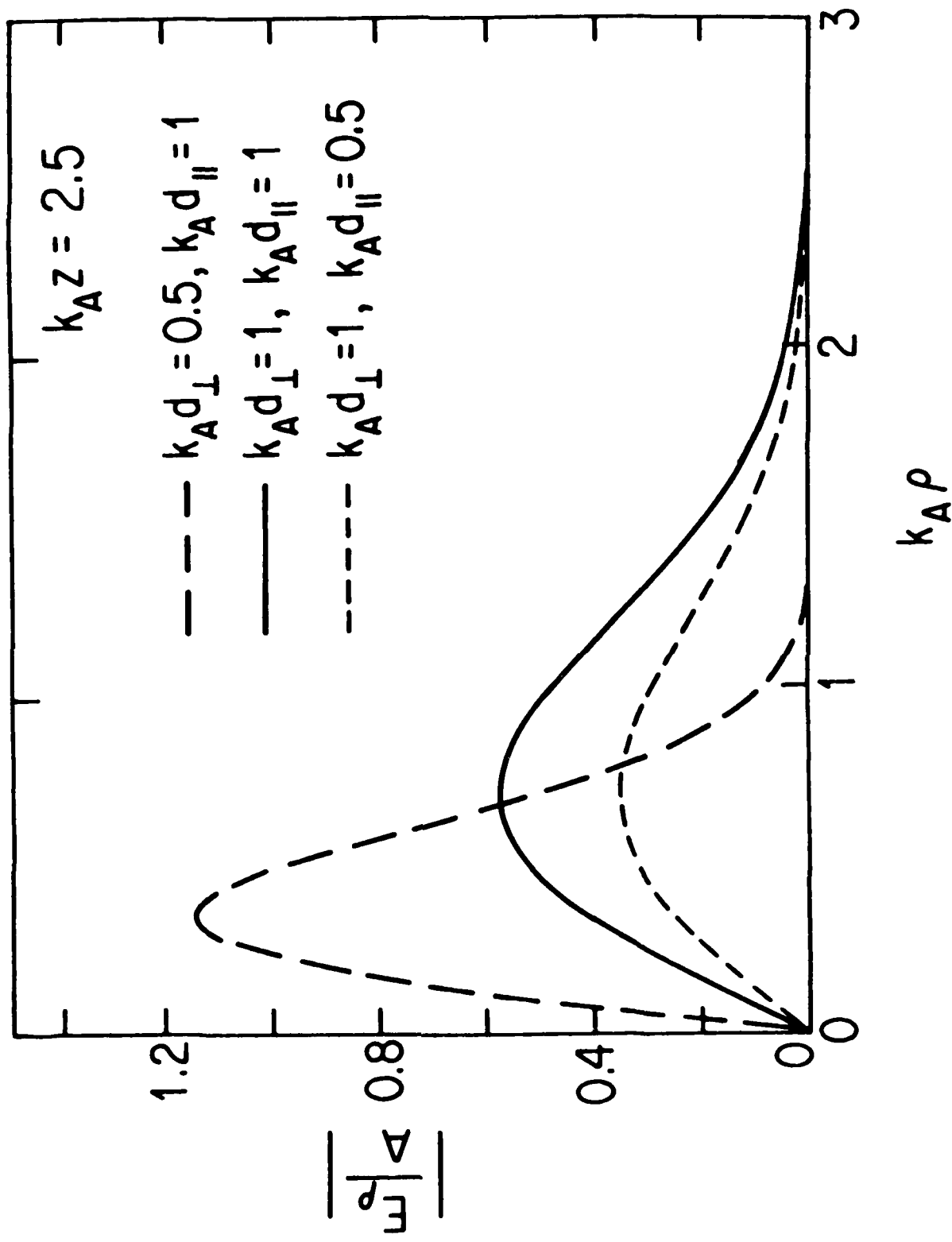


Fig. 7

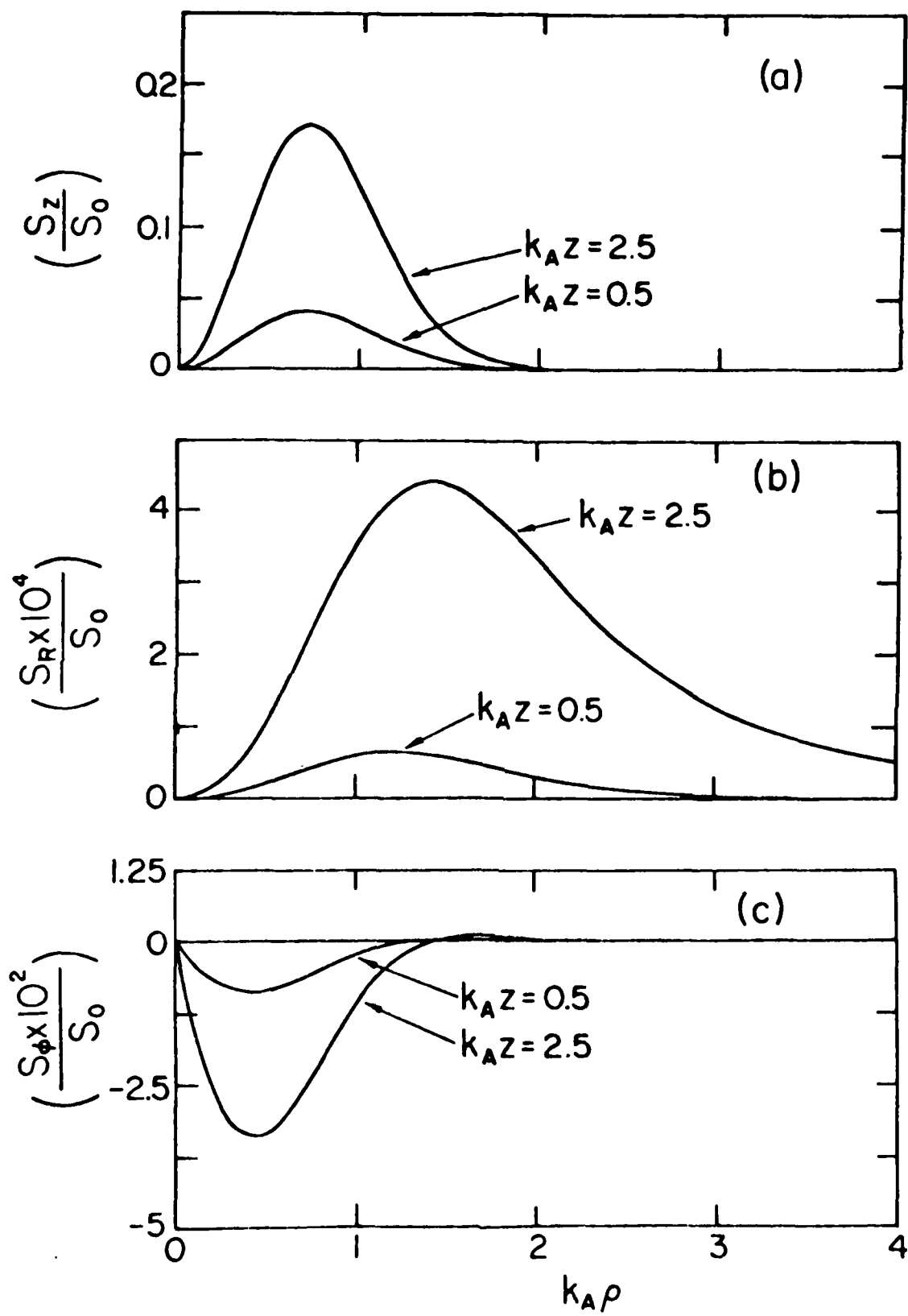


Fig. 8

6

PPG-808 "Experiments on Langmuir Collapse", A. Y. Wong, P.Y. Cheung, Int'l. Conf. on Plasma Physics, July (1984).

PPG-809 "Multichannel Far-Infrared Interferometer/Polarimeter", P.E. Young.

PPG-810 "The  $k = 0$  Mode Contribution in Periodic & Bounded Particle Simulation Codes", B. Lembège and J.M. Dawson.

PPG-811 "Observation of the Externally Excited Fast Magnetosonic wave via Collective Thomson Scattering", H. Park, W.A. Peebles, MC. Luhmann, Jr., R. Kirkwood, R.J. Taylor.

PPG-812 "Multichannel Scattering Studies of the Spectra and Spatial Distribution of Tokamak Microturbulence", D.L. Brower, W.A. Peebles, N.C. Luhmann, Jr., R.L. Savage, Jr., submitted to Phys. Rev. Lett. in July 1984.

PPG-813 "Thermalization of neutral-beam-injected ions by lower hybrid waves in Jupiter's magnetosphere," D. D. Barbosa, August (1984).

PPG-814 "Nonlinear Evolution of Slow Waves in the Solar Wind," T. Hada & C. F. Kennel, August, 1984.

PPG-815 "Technical Assessment of the Critical Issues and Problem Areas in High Heat Flux Materials and Component Development, Volume II," M. A. Abdou, et. al., June, 1984.

PPG-816 "Volume III: Strategies for International Collaborations in the Areas of Plasma Materials Interactions and High Heat Flux Materials and Component Development," W. B. Gauster, et. al., January, 1984.

PPG-817 "Raman Backscatter Below the Absolute Threshold," F. F. Chen, August, 1984.

PPG-818 "Boston Abstracts for the 1984 A.P.S. Meeting," August, 1984, S.T. Ratliff.

PPG-819 "Beat Wave and Surfatron Accelerator of Particles", August, 1984. J.M. Dawson.

PPG-820 "Prospects of the Surfatron Laser Plasma Accelerator", T. Katsouleas, C. Joshi, W. Mori, J.M. Dawson, June, 1983.

PPG-821 "FINESSE: A Study of the Issues, Experiments & Facilities for Fusion Nuclear Technology Research and Development, Interim Report," M. Abdou, et al., September, 1984.

PPG-822 "A Quarter Century of Collisionless Shock Research," C. F. Kennel, J. P. Edmiston, T. Hada, September (1984).

PPG-823 "Stability of Ballooning Modes in an Axisymmetric Mirror by a Hot Electron Ring and a RF Electric Field," H. Sanuki, G. J. Morales & B. D. Fried, October (1984).

PPG-824 "Resonant Instability Near the 2-Ion Cross-over Frequency in the Io Plasma Torus," R. Thorn & J.J. Moses, submitted to JGR, October, 1984.

PPG-825 "Generation of Lower Hybrid Noise by Superthermal Cross-Field Ion Currents," D. D. Barbosa, October (1984).

PPG-826 "Quasi-Thermodynamic Prediction of Hydrogen Re-emission from Titanium Films," Y. Hirooka, R. W. Conn, D. M.

**END**

**FILMED**

**2-85**

**DTIC**